Geologia USP
Série Científica

https://doi.org/10.11606/issn.2316-9095.v25-228297
Revista do Instituto de Geociências - USP
Geol. USP, Sér. cient., São Paulo, v. 25, n. 4, p. 55-71, December, 2025

Interaction of magmatic and meteoric water during barite crystallization in the Seival area (Cu), epithermal deposit from the Camaquã Basin, Neoproterozoic Dom Feliciano Belt of southern Brazil

Interação de água magmática e meteórica durante a cristalização de barita na área do Seival (Cu), depósito epitermal da Bacia do Camaquã, Cinturão Dom Feliciano, Neoproterozoico do sul do Brasil

Rodrigo Winck Lopes[1,2,3], André Sampaio Mexias[2], Christophe Renac[3], Márcia Elisa Boscato Gomes[2], Eduardo Fontana[4], Aurélie Barats[3]

[1]Universidade Federal da Bahia, Instituto de Geociências, Rua Barão de Geremoabo, s/n°, CEP: 40170-290. Salvador, BA, BR. (rodrigolopes@ufba.br)
[2] Universidade Federal do Rio Grande do Sul, Instituto de Geociências, Porto Alegre, RS, BR. (andre.mexias@ufrgs.br; marcia.boscato@ufrgs.br)
[3] Université Côte d'Azur, Géoazur, Sophia Antipolis, FR. (christophe.renac@unice.fr; aurelie.barats@unice.fr)
[4] Universidade Federal dos Vales do Jequitinhonha e Mucuri, Centro de Geociências, Diamantina, MG, BR. (eduardo.fontana@ict.ufvjm.edu.br)

Received on August 25, 2024; accepted on November 19, 2025.

ABSTRACT

Barite is a common gangue mineral of the low-temperature in hydrothermal systems. In the Seival area, the relative chronology of minerals indicates that barite, calcite, and minor hematite are associated with the low-temperature hydrothermal stages (< 157 °C) of an epithermal mineralization from the Camaquã Basin, Neoproterozoic Dom Feliciano Belt. Previous interpretations of geochemical data have suggested that the Cu enrichment in sulfides was related to albitization and chloritization, but not determined the origins or crystallization conditions of barite. The Ba and S content and their precipitation conditions were examined, and a lower Ba content was observed in the altered plagioclase with an albite composition than in the less altered portion with an andesine--labradorite composition. In addition, and rare earth elements (REEs) analysis of barite and plagioclase suggest that elementary composition of barite in Seival area came from volcanic material (magmatic) with influence of meteoric water rather than seawater. The different REEs patterns of barite show two groups related to two magmatic sources of REEs. These different sources of S, Ba, and REEs have been interpreted as dominant alteration of local volcanogenic rocks as the pyroclastic rock and andesite lava flows or less probably lamprophyric dike.

Keywords: REEs geochemistry; Hydrothermal alteration; Mineralization; Mantiqueira Province; Hilário Formation.

RESUMO

A barita é um mineral de ganga comum em sistemas hidrotermais de baixa temperatura. Na área do Seival, a cronologia relativa dos minerais indica que a barita, a calcita e a pouca hematita estão associadas aos estágios hidrotermais de baixa temperatura (< 157° C) de uma mineralização epitermal da Bacia do Camaquã, Cinturão Dom Feliciano, Neoproterozoico. Interpretações anteriores de dados geoquímicos sugeriram que o enriquecimento de Cu nos sulfetos está relacionado à albitização e à cloritização, mas não determinam as origens ou as condições de cristalização da barita. O conteúdo de Ba, S e suas condições de precipitação foram examinados e foi observado um conteúdo menor de Ba no plagioclásio alterado que possui composição de albita, do que na

porção menos alterada que possui composição de andesina-labradorita. Além disso, a análise de elementos de terras raras (ETRs) de barita e plagioclásio sugere que a composição elementar da barita na área de Seival veio de material vulcânico (magmático) com influência de água meteórica em vez de água do mar. Os diferentes padrões de ETRs da barita mostram dois grupos relacionados a duas fontes magmáticas de ETRs. Essas diferentes fontes de S, Ba e ETRs foram interpretadas como alteração dominante de rochas vulcanogênicas locais, como rocha piroclástica e fluxos de lava andesítica ou, menos provavelmente, dique lamprofírico.

Palavras-chave: Geoquímica de ETRs; Alteração hidrotermal; Mineralização; Província Mantiqueira; Formação Hilário.

INTRODUCTION

The hydrothermal alteration process occurs through the percolation of hot fluids promoting mineralogical, chemical, and textural changes in the host rock. These fluids might have different origins and might be eventually associated with to mineralization (Pirajno, 2009; Sillitoe, 2010; Fulignati, 2020). In particular, the crystallization of barite ($BaSO_4$) is associated with low-temperature fluids (< 150 °C; Hanor, 2000). The extremely low solubility of barite (Deer et al., 2013; Jamieson et al., 2016) makes it resistant to weathering. Consequently, this mineral might help in the reconstruction of fluid circulation at low-temperature of crystallization. The crystallization of barite is promoted by fluids with barium and sulfate ions that are the product of alteration of barium-rich feldspar and pyroxene (Sorrell, 1962; Green, 1980; Mehnert and Büsch, 1981; Chang et al., 1996; Deer et al., 2013), and oxidation of some sulfides (Brimhall and Crerar, 1987; Vaughan and Craig, 1997) or sulfates from seawater (Goldberg et al., 1969; Piper, 1974; Michard et al., 1984; Elderfield, 1988; Martin et al., 1995). The barite vein or disseminated in the Camaquã mine is associated with Cu-Pb-Zn-rich sulfides related to late-magmatic to low-temperature hydrothermal stages from a distal-epithermal system (Bettencourt, 1976; Remus et al., 2000; Toniolo et al., 2004; Renac et al., 2014).

The mineralization has a structural direction similar to regional shear zones in a post-collisional setting, as described by Lopes et al. (2018). The Cu mineralization at the Seival area was interpreted as epithermal deposits (Fontana et al., 2017) related to andesitic to trachyandesitic dikes. The hydrothermal stage characterized by albitization and chloritization (Fontana et al., 2017, 2019) is associated with the circulation of fluids and a structural control (Lopes et al., 2019) in favor of Cu-deposition. Lopes et al. (2019) suggest that Cu enrichment and barite crystallization are related to the pervasive and large/late stage of the hydrothermal alteration with influence of regional structures. Like in many places of the world (Pirajno, 2009; Sillitoe, 2010; Fulignati, 2020), the percolation and the mixing of the different fluids, magmatic then meteoric, are associated to a porphyry-epithermal hydrothermal system.

In the Seival area, barite occurs after albitization (250 to 650 °C) of andesine-labradorite and represents the latest aqueous-fluid circulation (<250 °C) interpreted as low-temperature meteoric fluids (Hanor, 2000). In the literature, hydrothermal-volcanic systems with barite and calcite may have different trace element and rare earth element (REEs) concentrations. However, few studies have addressed the origin of barite and its formation conditions (Guichard et al., 1979; Michard, 1989; Barrett et al., 1990; Martin et al., 1995). Major and trace elements could contribute to the understanding of Ba and S sources related to alteration of surrounding volcanogenic rocks or seawater (e.g. Guichard et al., 1979; Morgan and Wandless, 1980; Jurkovic et al., 2010; Zarasvandi et al., 2014) as shown by REEs patterns from continental-hydrothermal to barite-related seawater (Michard, 1989) and the possible influence of a regional aquifer. The present study proposes to reconstruct the hydrothermal, magmatic and meteoric origin of barite precipitation by analyzing the major elements and REEs contents in barite. These interpretations may be useful to understand the hydrothermal evolution and water-rock interactions in barite crystallization. The high REEs concentration in barite could be used as an exploration guide for base metal deposits in an epithermal context.

GEOLOGICAL SETTINGS

Regional geology

The Neoproterozoic/Early Paleozoic Mantiqueira Province (MP) (900 – 480 Ma) is located in southeastern and southern Brazil and extends into Uruguay (Almeida and Hasui, 1984; Almeida et al., 2000; Brito Neves et al., 2021) (Figure 1A). This province was formed during the Western Gondwana orogeny, called Brazilian in Brazil and Panafrican in Africa. Its southernmost part has been subdivided

into two geotectonic units (Philipp et al., 2016; Hueck et al., 2018) that were fused during the collision between the La Plata and Kalahari cratons: (i) the Nico Perez Terrane; and (ii) the Dom Feliciano Belt (Chemale Jr., 2000; Hartmann et al., 2007; Oyhantçabal et al., 2011; Philipp et al., 2016) (Figure 1B). The Camaquã Basin (610 – 550 Ma; Chemale Jr., 2000; Paim et al., 2000, 2014) (Figure 1C) developed during the final evolution of the Dom Feliciano Belt (Chemale Jr., 2000; Oyhantçabal et al., 2011; Oriolo et al., 2018) and hosts several important mineral deposits, such as the Cu (Au) and Pb-Zn (Cu, Ag) Camaquã Mine (Remus et al., 2000; Camozzato et al., 2014; Renac et al., 2014; Pereira et al., 2021) and the Cu-Ag Seival area (Reischl, 1978; Lopes et al., 2014).

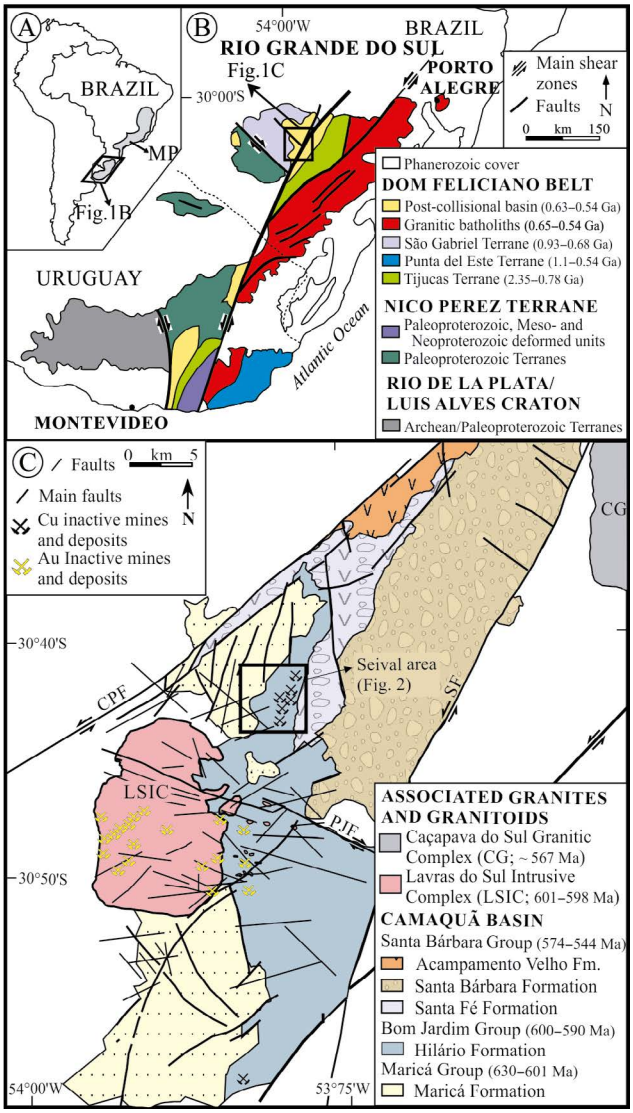

MP: Mantiqueira Province; LG: Lavras do Sul Intrusive Complex; CG: Caçapava do Sul Granitic Complex; CPF: Cabritos-Perau Fault; SF: Segredo Fault; PJF: Palma-Jacques Fault.
Modified from: (B) Hartmann et al., 2007; Oyhantçabal et al., 2011; Philipp et al., 2016; (C) Wildner et al., 2006; Gastal et al., 2015.

Figure 1. A) Southern portion of the Mantiqueira Province localization in South America; B) Geotectonic units of the 'Rio Grande do Sul' and Uruguay shields. C) Geological map of the Camaquã Basin and associated granites and granitoids with around twenty Au, Au-Cu, Cu, and Cu-Ag deposits.

The Seival area hosts a series of volcanogenic rocks associated with the Hilário Formation (600 – 590 Ma; Janikian et al., 2012) of the Bom Jardim Group (Lima et al., 2007; Janikian et al., 2008, 2012), which are locally associated with the Lavras do Sul Intrusive Complex through a porphyry-epithermal system (Bongiolo et al., 2011; Lopes et al., 2018). The Lavras do Sul Intrusive Complex hosts about twenty Au, Au-Cu, Cu and Cu-Ag deposits with phyllic and intermediate argillic halos around quartz veins (601 – 598 Ma; Gastal et al., 2006, 2015; Liz et al., 2009; Bongiolo et al., 2011) and represents the porphyry portion. In the Seival area, epithermal portion, the fractures and dikes of the Hilário Formation were associated with tectonic reworking related to shear zones and deformation episodes that allowed the development of intense fracturing (Lopes et al., 2018) and, consequently, fluid percolation (Fontana et al., 2017). Lopes et al. (2018) indicated that ore deposition is related to the development of these brittle shear zones with NE-SW and NW-SE directions in the Dom Feliciano Belt. In addition, the mineralized rocks have NE-SW directions and barite veins occur mainly in fractures with N-S directions. The volcanogenic rocks and dikes with andesitic to trachyandesitic compositions (Lopes et al., 2014) of the Seival area (Figure 2) host six Cu-Ag deposits and several occurrences surrounded by extensive hydrothermal halos with propylitic and argillic alteration. The approximate total reserve has been estimated at ~ 0.2 million tons with an averaged 1.4 wt% Cu and 10 – 70 ppm silver (Reischl, 1978).

Texture and mineralogy

Andesite lava flows, lapilli tuffs, and volcanic agglomerates (Lopes et al., 2014, 2019; Fontana et al., 2017; De Toni et al., 2021) represent the volcanogenic sequence. The pyroclastic materials and lava flows consist of vesicular andesitic rocks with phenocrysts of plagioclase and clinopyroxene dispersed in a trachytic groundmass with oriented plagioclase and disseminated pyroxene (Lopes et al., 2014). The lapilli tuffs are matrix-supported in a groundmass with crystals of plagioclase, pyroxene, quartz, and opaque minerals. Volcanic agglomerates contain rounded volcanic clasts. Dikes of andesitic and trachyandesitic compositions have subhedral phenocrysts of plagioclase and pyroxene in a trachytic groundmass with oriented plagioclase. Relicts of pyroxene phenocrysts are rare and most of them have been partially or completely replaced by clay minerals and calcite, sometimes keeping their original shape (Lopes et al., 2019). In addition, andesitic dikes have albitized plagioclase phenocrysts and some of them have the center portion with magmatic feldspar (andesine-labradorite) compositions.

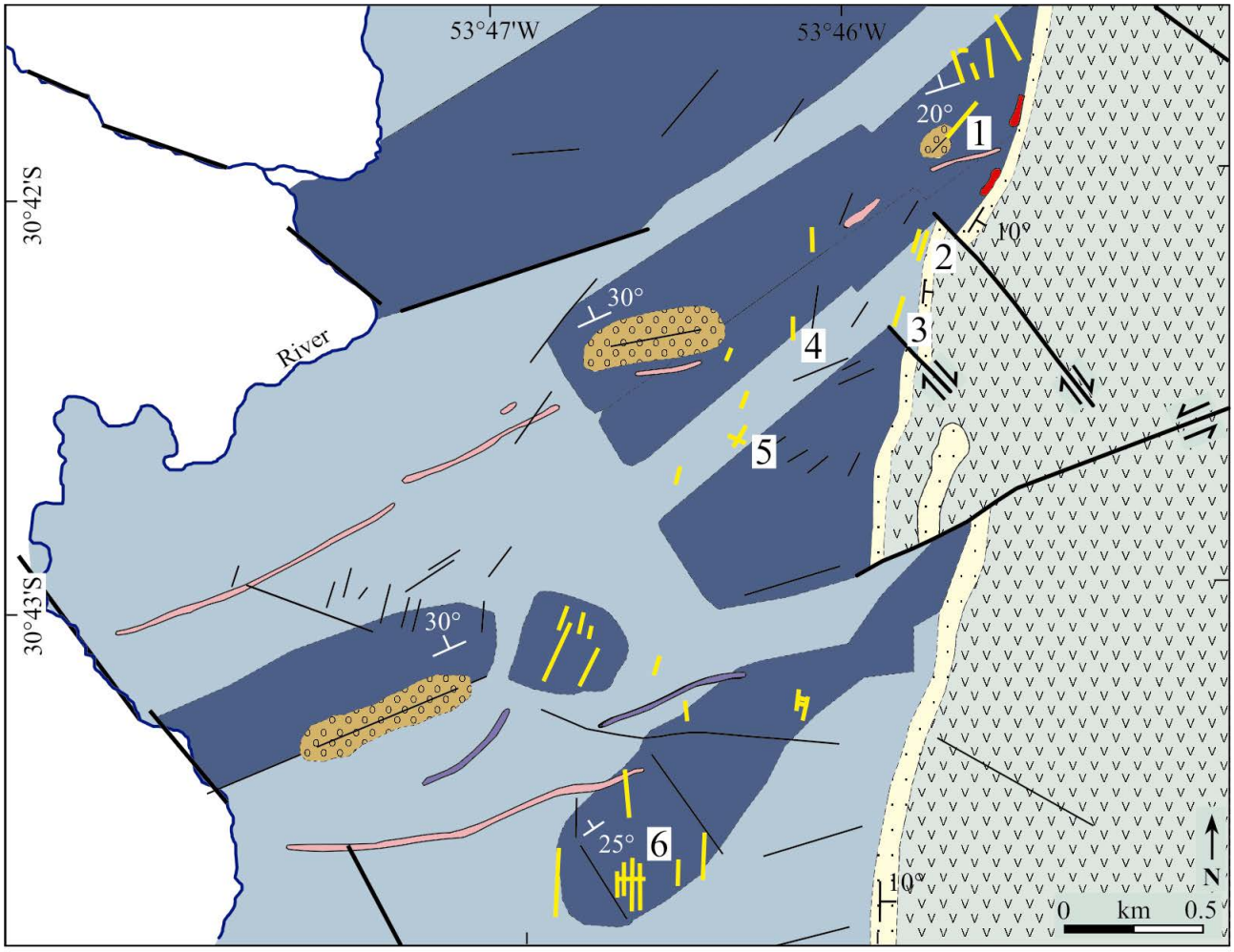

1: Barite; 2: João Dahne; 3: Morcego; 4: Meio; 5: Cruzeta; 6: Alcides. Modified from: Reischl, 1978; Lopes et al., 2014.

Figure 2. Geological map and six inactive mines location from Seival area. The sequence of lapilli tuffs, volcanic agglomerate, andesite lava flows and dikes with andesitic and trachyandesitic compositions (NE-SW direction) from Hilário Formation.

Relative chronology of alteration from Seival area

Alteration mineral is characterized as propilitic and the assemblages were crystallized through hydrothermal fluids with different temperatures (Table 1). A crystallization sequence and mineral assemblages of each thermal step of the alteration process were defined by petrography to understand the physic-chemical evolution of the hydrothermal system and the Cu-enriched stages.

Augite and less altered plagioclase with andesine-labradorite compositions (Lopes et al., 2019) were crystallized during magmatic crystallization. The deposition of primary sulfides represented by pyrite and chalcopyrite was considered as a late-magmatic hydrothermal alteration crystallized at ~ 350 °C (Fontana et al., 2017). In addition, calcite (Fontana et al., 2017), hematite, and quartz were associated with relicts or pseudomorphosis of pyroxene and plagioclase. Albitization (decalcification) of plagioclase, chloritization of pyroxene and destabilization of primary

Table 1. Crystallization sequence and mineral assemblages of magmatic (>650 °C), late magmatic and low-temperature (250 to > 650 °C) and low-temperature (~250 °C; <150 °C) characterized by Lopes et al. (2019).

Stage	magmatic	late magmatic to low--temperature	low-temperature	
temperature	>650 °C	250 to >650 °C	~ 250 °C	<150 °C
andesine-labradorite	—			
augite	—			
calcite		—	—	—
quartz		—	—	
hematite		—	—	
titanite		—	—	
epidote		—	—	
albite		—	—	
chlorite		—	—	—
chlorite/smectite (C/S)			—	
smectite				—
pyrite		—		
chalcopyrite		—		
chalcocite			—	
bornite			—	
barite				—

C/S: chlorite/smectite mixed-layers.

sulfides were associated with late magmatic and low-temperature alteration that crystallized at ~ 250 °C (Fontana et al., 2017; Lopes et al., 2019), while barite was crystallized at ~ 150°C (Hövelmann et al., 2010; Fontana et al., 2017). These interpretations did not indicate the source of barium and sulfate but emphasized crystallization related to fluid--rock interaction associated with an increasing proportion of meteoric water (Renac et al., 2014; Fontana et al., 2017) as supported by oxygen isotope analysis in albitized plagioclase, quartz, and calcite. The low temperature of barite was bracketed by the temperature of chloritization of pyroxene associated with calcite (Fontana et al., 2017), titanite and quartz formed between 130 and 280 °C (Lopes et al., 2014, 2019; Fontana et al., 2017) or chlorite/smectite mixed-layers ~ 250 °C (Kameda et al., 2011; Schleicher et al., 2012). The authors suggest that the alteration of magmatic feldspar, pyroxene and sulfide occurred through thermal changes (< 250 °C; Brimhall and Crerar, 1987; Vaughan and Craig, 1997; Dill, 2015; Vaughan and Corkhill, 2017) and the influx of meteoric water promoted by changes in chemical conditions (oxygen activity and pH changes) (Church and Wolgemuth, 1972; Ohmoto, 1972; Chiba and Sakai, 1985; Hanor, 2000). The association of chlorite and barite (Lopes et al., 2019) in Cu-sulfide mineralized fractures suggests a low-temperature crystallization of barite below 157 °C (chlorite thermometer based on Inoue et al., 2009; Lopes et al., 2019) for the Seival area. This temperature range is similar to those estimated for epithermal deposits from the Camaquã Basin by oxygen isotopes and fluid inclusions (115 – 125 °C: e.g. Cerro dos Martins; Toniolo et al., 2004) and 80 – 180 °C (e.g. Camaquã Mine; Bettencourt, 1976; Ronchi et al., 2000; Renac et al., 2014).

MATERIALS AND METHODS

The six outcrops with mineralization and their drill-core samples consist of volcanogenic rocks with hydrothermal alteration. The samples of barite samples are used in this study come from veins hosted in the lapilli tuffs and andesite lava flows from the Barite Mine location (Fontana et al., 2017; Lopes et al., 2019). Grain mounts and thin sections of barite were used for petrography and Electron Microprobe (EMPA) analysis.

To estimate the source of major elements for barite crystallization, major and trace elements were analyzed in plagioclase and barite samples using a CAMECA SXFive EPMA at the Geoscience Institute (Universidade Federal do Rio Grande do Sul, Brazil). Plagioclase analyses were performed using a 5 μm defocused beam, 15 kV and 10 nA (peak counting time 10 s and two background measurements of 5 s). Barite analyses were performed using a LPET detector with a 5 μm defocused beam (15 kV, 100 nA, peak and background counting times of 30 and 10 s, respectively). The measured X-ray intensities were ZAF corrected. The errors related to SiO_2, TiO_2, Al_2O_3, FeO, MnO, MgO, CaO, Na_2O, K_2O, BaO, SrO, CuO, and SO_3 weight percent vary from 0.01 – 0.05 (2 σ). The detection limits of Ba in atomic weight percent vary from 206 – 209 ppm (0.0002 %,

n= 33) with standard errors of 0.02 % (2σ) on consecutive measurements in samples.

The REEs contents were determined in concentrates of barite veins. Barite (500 – 250 mg) was melted into a Pt-crucible following Barbieri et al. (1982) and Breit et al. (1985) protocol. The barite (500 – 250 mg) mixed with Na_2CO_3 (5 – 2.5 g) was loaded (20 mL crucibles) with an addition of 1 mL Lithium-Iodide (LiI), to enhance the recovery of the fused material., The LiI was removed by evaporation during the melting process. The mixture was heated in a muffle furnace (1100 °C) for 10 hours. The cooled material was ground to a very fine powder using an agate grinder. The powder was dissolved in a cleaned Teflon beaker in distilled water (UHQ). The residues (Na_2CO_3 and $BaCO_3$) and sulfate-free solutions were heated in 10 mL of HCl and then evaporated to dryness and dissolved in HNO_3 (1 mol L^{-1}). The dissolved material was passed through C_{18} Sep-Pak cartridges (Shabani et al., 1992) to reduce the amount of barium and strontium. In this resin, all of the barium would be transported through the column without being bound to the bis (2-Ethylhexyl) orthophosphoric acid. The cartridge was rinsed (10 mL of 0.01 mol L^{-1} HCl) then its content eluated with HCl (30 mL, 6 mol L^{-1}). The use of a Ba-REEs spiked solution (1.5 mg L^{-1}) allowed the determination of an optimal elution time for a REEs recovery of 87 %.

The digested solutions were analyzed for their REEs contents (^{139}La to ^{175}Lu) by ICP-MS (Elan DRCII, Perkin Elmer) at GEOAZUR laboratory (Université Côte d'Azur, France) using an external calibration and internal standards (Re and Ge selected according to the targeted mass). Quantification limits were less than 50 ng L^{-1}. Spectral interferences in the mass spectrum can occur due to the formation of oxides in the plasma (Longerich et al., 1987; Jarvis et al., 1989, 1992; Smirnova et al., 2006; Zhao et al., 2019). Formation lead to significant interferences of intermediate REEs (Dulski, 1994; Aries et al., 2000; Raut et al., 2005a, 2005b). Therefore, the matrix was removed by resin separation (see above) and oxide production level was limited. The percentage of barium oxide was checked daily during the daily performance optimization of the ICPMS before the analyses. This percentage is always below 3%, usually around 2%. La to Sm elements were considered as Light Rare Earth Elements (LREEs), and Eu to Lu as Heavy Rare Earth Element (HREEs). Elemental concentrations were expressed in ppm (mg kg^{-1}) and normalized to chondrite values (McDonough and Sun, 1995) using Microsoft Excel and a graph editor.

Chemical Data treatment

The chemical compositions of minerals (EPMA) and whole-rocks (ICP-MS) were further used in mass balance calculations to estimate the volume of volcanic rocks and seawater required to precipitate one mole of barite. In addition, a mass balance calculation using the Geobalance spreadsheet (Li et al., 2020) was used with REEs compositions of barite and several volcanic rocks of the area to estimate the contribution of each volcanic rock of the area in the barite crystallization. Twenty-four mixtures with two to five end members (meteoric water, RFM48, RFM 68, AN122B, and LP225) were tested (see Methodology). These mass balance calculations were performed without Eu and Yb concentrations due to possible overestimation of Eu content with barium oxide residues and unknown partition coefficient (Kd) of Yb between barite and brine. In this mass balance, the REEs compositions of whole-rocks from the Seival-Camaquã area, reported in Lima and Nardi (1998) and Lopes et al. (2014) were used as input values. In addition, local rocks such as pyroclastic rocks (RFM48), andesitic lava flows (RFM68), andesitic dyke (AN122B) and lamprophyric dyke (LP225), and REEs from barite. A standard deviation of 10% and a Monte Carlo simulation was performed. Mass balance calculations of REEs contents allowed the estimation of the contribution of the volcanic sequence (RFM48, RFM68 and AN122B) and the lamprophyre dike (LP225; Gastal et al., 2006; Almeida et al., 2012) to barite formation.

RESULTS

Cu-mineralization and barite veins

The Cu mineralization, in the Seival, is found along faults (Figure 3A) and within fractures where chalcocite veins are present or on superficially altered rocks with malachite and occasionally azurite (Figure 3B). The mineralized rocks have several colors indicating different alterations (Figure 3C): light green represents the chlorite composition; the dark purple characterizes the association of chlorite and hematite (Figure 3D), verified by XRD. The chalcocite (Figures 3E and 3F) and bornite (Figure 3G) are transformed into malachite in the mineralized zones. The Barita Mine is the main location of gangue minerals as barite and calcite in the form of veins or veinlets associated to Cu mineralization, outside the Barita Mine, barite veins are smaller and less numerous.

Characterization of Barita Mine area

In the Barita Mine area (Figure 4A), a significant number of barite veins were observed. The Cu-Ag mineralization, indicated by white dashed lines (Figure 4A), occur in the volcanogenic sequence mainly along NNE to NNW subvertical structures in the form of veins and disseminated within the host rocks matrix. The mineralized structures within the host rocks 2 to 4 meters in width (Figures 4B and 4C). These structures contain chlorite and Cu-sulfides or malachite (Figure 4D), and a significant quantity of barite and calcite veins from millimeter to centimeter in size. These barite veins are found in the subvertical fault plans, e.g. N10°E, N10°W and N40 – 60°E with dip angle ranging from 70 – 88°.

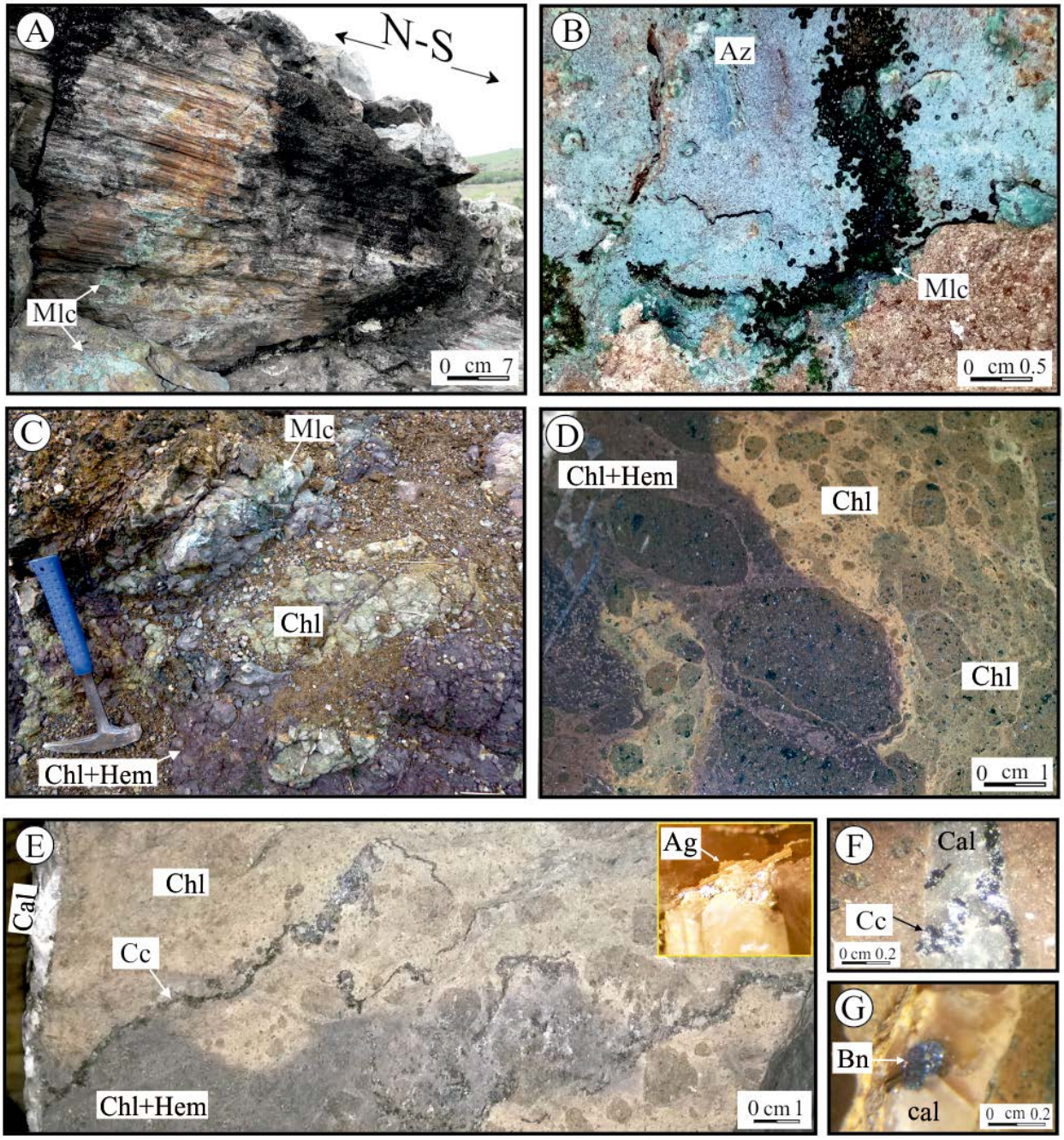

Mlc: malachite; Az: azurite; Chl: chlorite; Hem: hematite; Cal: calcite; Cc: chalcocite; Ag: native Silver; Bn: bornite.

Figure 3. Photographs of the mineralization from the Seival area. (A) Slickenlines filled by hematite and malachite in a fracture zone from Alcides Mine; (B) Botryoidal malachite and azurite in the fractured volcanic rocks from Alcides Mine; (C) Alteration with chlorite and chlorite + hematite in mineralized rocks from Barita Mine; (D) Detail of the hydrothermal alteration indicated by several colors in lapilli tuffs from Meio Mine; (E) Alteration with chlorite and chlorite + hematite cross-cut by chalcocite vein. Detail of native Silver (Ag) disseminated in lapilli tuffs from Meio Mine; (F) Detail of calcite + chalcocite vein; (G) Detail of calcite + bornite vein.

Characterization of barite

The barite and calcite veins and veinlets in the hydrothermal zone exhibit hematite, chlorite, and chlorite/smectite mixed-layers (C/S) halos (Figure 5A). These iron- clay-rich halos contain scarce disseminated crystals of Fe-Cu and Cu-rich sulfides minerals as bornite and chalcocite. Stereo microscopy has revealed white to pinkish colors, aggregates of tabular and prismatic shapes and subhedral to euhedral habits in the barite from veins and veinlets. Special attention was given to barite crystals and their inclusions. In (Figure 5B) these mineral inclusions are calcite, sulfides and hematite. Moreover, microscopic observations of calcite-rich veins with quartz veins and a smaller proportion of barite and hematite in calcite.

The veins of barite and calcite forms a mineral assemblage and calcite is considered as last crystallized vein

Mlc: malachite; Chl: chlorite.

Figure 4. Photographs of the Barita Mine, the main barite location from Seival area. A) A view of deposit and mineralized structures; B) Mineralized structure with indication of NE-SW and ~ N-S oriented faults; C) Mineralized rock with chlorite veins and malachite in lapilli tuffs; D) Mineralized rocks with disseminated malachite in the rock matrix. White dashed lines: mineralized structures.

mineral due to the cross-cut relation (Figure 5C). Calcite occurs within joints of barite crystals as inclusion, in the contact between barite vein and host rock (Figure 5D). Furthermore, calcite veins are associated with bornite-chalcocite, hematite, and scarce micrometer size white mica. Chalcocite grains fill vesicles and the volcanogenic rock matrix (Figure 5E). The chalcocite grains also were concentrated in the calcite and along the contact between barite and calcite veins (Figure 5F). On fractured plans exposed to weathering or rainfall runoff the recent weathering of Cu-sulfides produced malachite and azurite (detail of Figure 4D).

Ba content in plagioclase

Plagioclase crystals were analyzed in preserved not albitized portion and in the albitized portion. We define albitization process as leaching or loss of Ca (decalcification) from part or all of the plagioclase. There is no direct precipitation of albite, only a loss of Ca, changing the composition of the andesine~labradorite to albite. The EPMA analysis

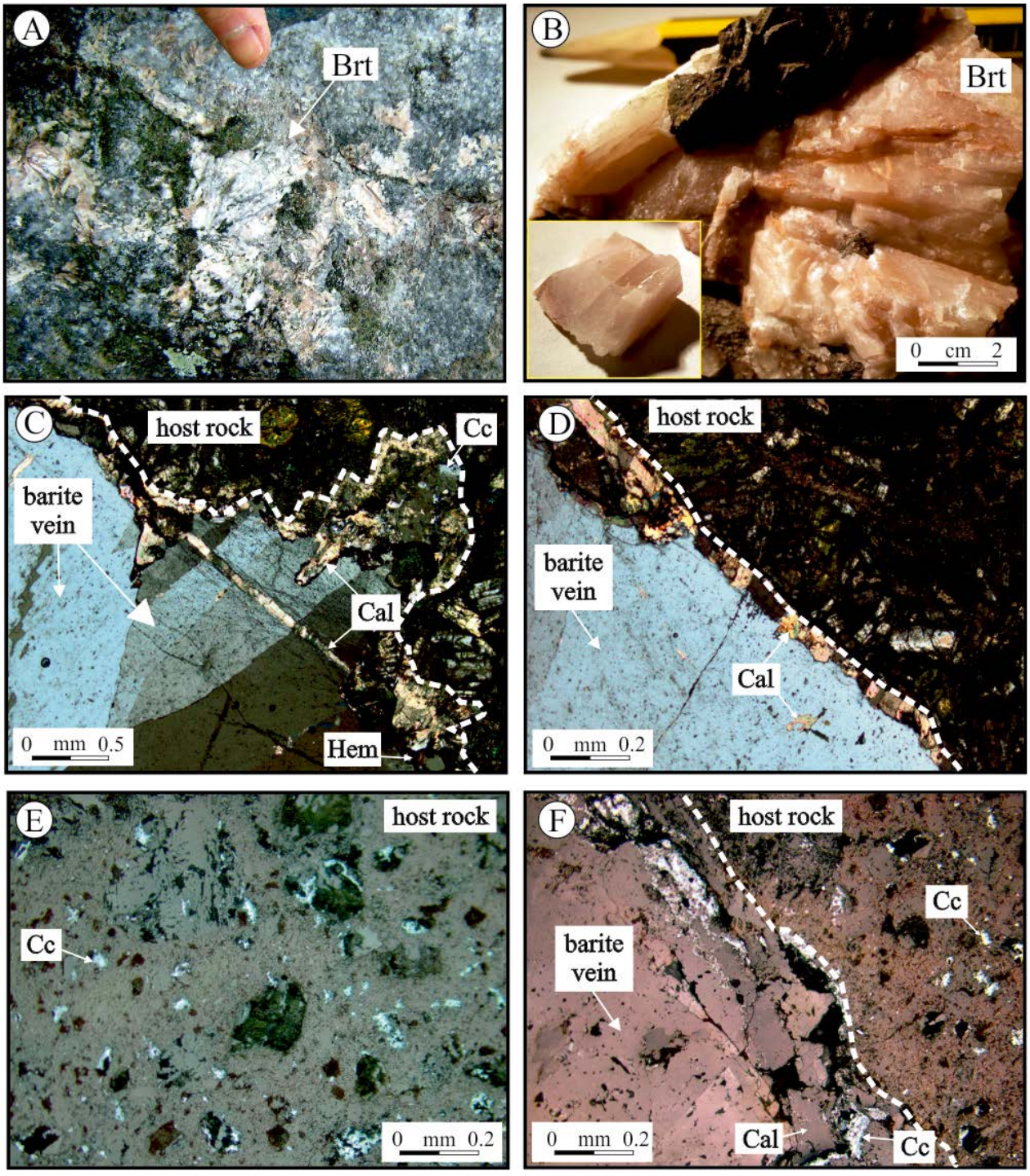

Brt: barite; Cal: calcite; Cc: chalcocite; Hem: hematite.

Figure 5. Photos of the barite (A and B) and photomicrograph of the lapilli tuffs from Barite Mine (C and D - cross-polarized light; E and F - reflected light). (A) White to pinkish barite and aggregates of tabular and prismatic crystals shapes; (B) Barite sample analyzed and detail (inset) of a crystal separated from Barita Mine; (C) Barite vein cross-cut by calcite vein; (D) Barite vein with inclusion of calcite; (E) Chalcocite disseminated in lapilli tuffs groundmass; (F) Association of calcite vein and chalcocite. White dashed lines: contact between host rock and barite vein.

of major element compositions of magmatic (andesine-labradorite; Figure 6A) and albitized feldspars (albite; Figure 6B), showed variable Ba contents. The andesine-labradorite contained 0.11 – 0.14 atomic wt % of Ba while the albite contained less than 0.02 atomic wt % (Supplementary document - Appendix A).

Ba content in barite veins

Barium concentration in barite veins varied from 56.87 – 59.10 atomic wt %, S contents from 13.08 – 14.05 atomic wt %, O contents from 26.42 – 27.94 atomic wt %, and low contents of Sr and Na (Supplementary document

- Appendix B). The low Sr concentrations (0.02 – 1.01 atomic wt %) indicate a barite-celestine solid solution series. Trace elements in the barite are dominantly composed by Na (0.02 – 0.16 atomic wt %) alongside trace amounts of Si, Mg, Al, K, Ca, Ti, Cu, Mn, and Fe contents, most probably related to microscopic inclusion of silicates.

REEs content in barite veins

The total concentrations of REEs in barite (ΣREEs normalized in ppm; Supplementary document - Appendix C) vary from 3573 – 10293 ppm (927 – 4387 ppm, without Eu content). The LaN /LuN normalized ratios varied from 0.04 – 0.11. Based on the results, we separated the barites into two groups. The REEs contents of the Group 1 is due to different samples with similar patterns (brt2 and brt3). In contrast, the REEs patterns of the Group 2 show less LREEs (Ce, Pr, and Nd) and HREEs (Dy and Er) than Group 1. In addition, Group 1 barite has a higher REEs contents that can indicate a different source.

DISCUSSION

Hydrothermal environment of barite crystallization

Barite crystallization generally occurs through two processes. The first is the addition of sulfur-rich hydrous or gaseous fluid to an aqueous phase rich in Ba ions. The second involves adding Ba ions to a sulfate-rich fluid (e.g. Hanor, 2000). As early presented, the veins found in the fractured zone infilled with barite and calcite represent a mineral assemblage, as Fontana et al. (2017) have pointed out. Instead, they suggest an influx of meteoric water. The inclusions chalcocite-bornite or specular hematite in barite crystals display redox changes of the aqueous fluids marked by dominant HS- species changing to an increasing proportion of SO_4^{2-} species related to the rise of oxygen fugacity (Fontana et al., 2019). The precipitation of a large amount of barite relies to high concentrations of Ba^{2+} and SO_4^{2-} ions in water (< 2.5 x 10-5 mol.kg^{-1} equivalent to 3.4 mol.kg^{-1} of Ba^{2+} and 2.4 mol.kg^{-1} of SO_4^{2-}) and very low equilibrium constants (25 to 100 °C: $10^{-9.48}$ to 10^{-10}: Lawrence Livermore National Laboratory, thermodynamic database). However, if the barite may be easily crystallized in large volumes, it is likely that the source of barium and sulfur is associated with volcanogenic rocks (Chow and Goldberq, 1960; Guichard et al., 1979; Ehya, 2012) or seawater (Martinez-Ruiz et al., 2020). In the former scenario , barite crystallization could to be related to the plagioclase albitization process (Ba source) and destabilization of primary sulfides (S source) in a shallow environment with a significant contribution of meteoric fluid as evidenced by an increase of the oxygen fugacity. In the second case, barium and sulfur occur commonly as ion species in seawater.

Estimates of altered whole-rocks and seawater needed for barite crystallization

The change of barium content in the andesine-labradorite (0.12 atomic wt %) to albite, below the detection limit of barium, indicates leaching of barium from magmatic feldspars during albitization. Barium and sulfur contents of magmatic feldspars (Lopes et al., 2019) and altered whole-rocks (Lopes et al., 2014) from the Seival area and seawater (Hogdahl, 1968) were used to calculate how much volume of these materials is required to form barite. For magmatic feldspars, the mass of barium in the andesine-labradorite was estimated to be 0.322 g of Ba in one mole of feldspar [= 0.12 atomic wt % (proportion of Ba in the andesine-labradorite) x 268.62 g.mol^{-1} (M(andesine))]. In one mole of barite, there was a mass of 137.32 g of ba-

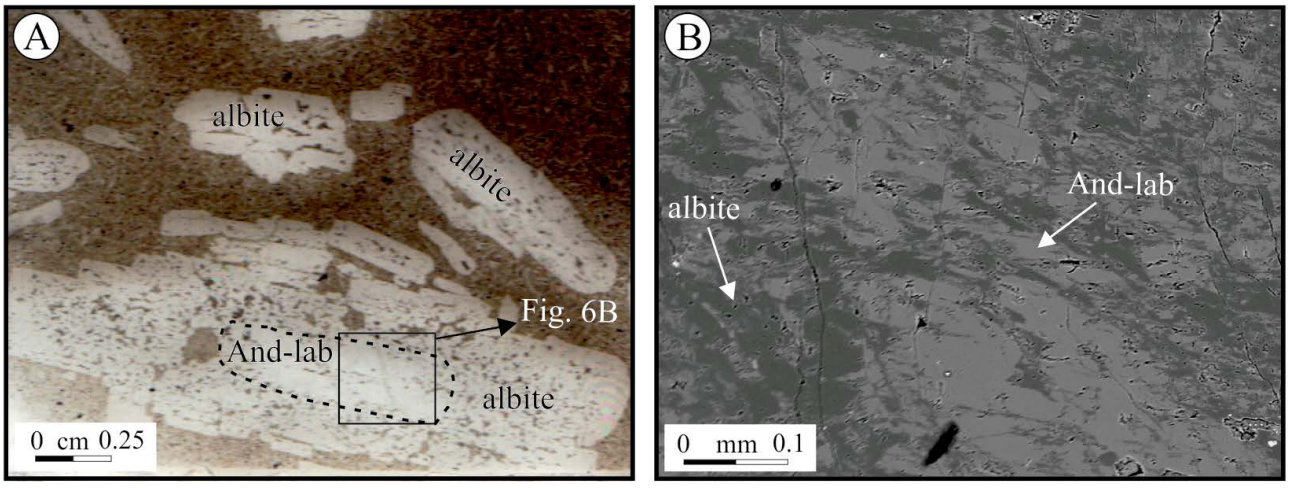

And-lab: andesine-labradorite.

Figure 6. Photo and micro photos of plagioclase in the thin section. (A) Parallel polars micro photo of igneous plagioclase phenocrysts from andesitic dike with phenocrysts of original plagioclase (andesine-labradorite) in the center and altered plagioclase (albite) in the boundaries; (B) Backscattered electron image showing a detail of the plagioclase with the central portion with andesine-labradorite and an altered portion of albite composition from andesitic dike.

rium [= 0.5884 (proportion of Ba in barite) x 233.39 $g.mol^{-1}$ (M(barite))]. To precipitate one mole of barite, 426 moles of feldspar (andesine) (= 137.32/0.32) would be required. These 426 moles of andesine represent 115 kg (= 426 mol x 268.62 $g.mol^{-1}$) which is equivalent to a volume of 4.41 x 10^{-2} m^3 of feldspar [=115 kg/2600 $kg.m^{-3}$ (the volumetric mass of andesine)]. In seawater, one mole of seawater contains of 1.44 x 10^{-4} to 5.58 x 10^{-4} g of Ba [= 0.0008 to 0.0031 (atomic wt %) x 18.01 $g.mol^{-1}$ ($M(H_2O)$)] (Hogdahl, 1968). A quantity of 2.46 x 10^5 to 9.53 x 10^5 mol of seawater [= 137.32/(1.44 x 10^{-4} to 5.58 x 10^{-4})] would be required to precipitate one mole of barite, which corresponds to a mass of 4.43 x 10^6 to 1.72 x 10^7 g of seawater [= (2.46 x 10^5 to 9.53 x 10^5) x 18.01 $g.mol^{-1}$]. Given a volumetric mass of seawater of 1025 $kg.m^{-3}$, a volume of 4.32 – 16.7 m^3 [= (4.43 x 10^6 to 1.72 x 10^7 g)/1025 $g.L^{-1}$] of seawater is required to precipitate one mole of barite. Similar to Ba, the mass of S in the altered whole-rocks (Lopes et al., 2014) from the Seival was used to estimate the amount of sulfide (in moles) required to produce one mole of barite (Supplementary document - Appendix C). These calculations revealed that 13 moles of whole-rock or (96.063 g of SO_4 in one mole of barite/ typical concentration of SO_4 in seawater 2.649 g. L^{-1}) or 36.26 L equivalent to 2014.66 moles (36.26 L x 55.55 mol. L^{-1}) of seawater would be needed to precipitate one mole of barite.

In each calculated case, the low concentration of Ba in feldspars and volcanic rocks and sulfur in seawater are the limiting concentrations to form barite. However, the comparison of the Ba and S components delivered by feldspars and seawater indicates that feldspar-whole-rocks supply for more Ba and S components than seawater. Consequently, one mole of barite is more easily precipitated from feldspar or whole-rock with feldspar and sulfide (4.41 x 10^{-2} m^3) than from seawater (4.32 – 16.7 m^3). The lack of the total amount of barite in the area, limits further interpretation, which consists of calculating the total volume of altered volcanic rocks in the area or the total volume of seawater circulation.

Source of rare earth elements in the barite

As mentioned in sections 5.1 and 5.2, barite crystallization occurs so simple that Ba and S can either come from the volcanogenic rock or from seawater incursion. Thus, the Therefore, REEs geochemistry in barite has been used in the literature to reconstruct the origin of trace elements in this mineral (e.g. Hogdahl et al., 1968; Guichard et al., 1979; Barrett et al., 1990; Martin et al., 1995; Ehya, 2012). The REEs analyses of barite (Group 1) from Seival area with Ce/La averaging 1.7 (not normalized calculi; Supplementary document - Appendix C) are similar to those measured in barite from continental areas (Guichard et al., 1979; Barrett et al., 1990; Martin et al., 1995) while lower Ce/La ~ 0.35 ratio barite would form in the absence of seawater contribution (Goldberg et al., 1969; Church and Bernat, 1971; Guichard et al., 1979) or precipitate from acidic waters (pH < 6; T > 230 °C) in submarine hydrothermal vents (Michard et al., 1989). These characteristics of Ce/La combined with stable-isotope interpretations (Fontana et al., 2019) suggest an influx of meteoric water in the Seival area or several types of magmatic rocks, continental or from submarine hydrothermal vents. Similar REEs distributions are found in various deposits as from Bahariya Oasis, southern Egypt (Baioumy, 2015). The high concentrations of REEs measured in the Seival area are interpreted as a product of hydrothermal alteration of volcanic rocks.

For the interpretation of fluid composition, REEs contents in water needs to be calculated. However, no experimental study has presented the partition coefficient of lanthanides in water in association with barite. However, numerous studies have been conducted on gypsum in volcanic lakes (Inguaggiato et al., 2015, 2017), seawater (Censi et al., 2004, 2017), the mixture of seawater and meteoric water in a volcanic context (Johannesson et al., 2017), or sulfate-rich fluids (Schijf and Byrne, 2004). The latest study on REEs partition coefficient (Kd) and sulfate is associated with gypsum crystallization in the brine of a volcanic lake (Inguaggiato et al., 2018). The REEs partition coefficient ($Kd_{REEs\ gypsum/brine}$) in the gypsum/brine system increased for La ($Kd_{La\ gypsum/brine}$ ca. 16) to Nd ($Kd_{Nd\ gypsum/brine}$ ca. 24) and decreased for Sm ($Kd_{Sm\ gypsum/brine}$ ca. 19) to Lu ($Kd_{Lu\ gypsum/brine}$ ca. 3). The Kd for Yb is currently unknown. Assuming a similar REEs partition coefficient for barite and gypsum, the REEs content in water varies from 473 – 834 and 241 – 443 ppm for Group 1 and Group 2 barite crystals, respectively. The ΣREEs was calculated without Europium due to a potential overestimation caused by BaO^+ (see Supplementary document - Appendix C). Based on the total concentration calculated of REEs contents in water and their elemental Ce/La ratios, it can be inferred that the origin of REEs for barite crystallization cannot be from seawater or evaporated seawater (Hogdahl, 1968; Li, 1982).

The high REEs content and REEs patterns of the fluid suggest that the REEs are derived from altered whole rocks. This may be the result of meteoric fluids (Fontana et al., 2017) oxidizing magmatic-volcanic rocks and dissolving H_2S which is then transformed into SO_4^{2-} (Seal II, 2006; Hoefs, 2009).

Except for HREEs (Yb and Lu), the REEs contents of water in equilibrium with Group 1 barite, including brt2 and brt3, produce REEs patterns (see Figure 7A) that are parallel to those of whole rocks or andesine-labradorite rich material., It is suggested that REEs present in fluids and barite are derived from altered volcanic rocks. Nevertheless, the overall concentration of REEs in water, excluding Eu, surpasses that of the encompassing whole-rocks as well as andesine-labradorite or albite (ΣREEs andesine-labradorite ~ 20 ppm and ΣREEs albite ~ 40 ppm; Lopes et al., 2019).

Considering previous calculations suggesting that meteoric-hydrothermal alteration of volcanic rocks is easier

than seawater circulation in the Seival area. All calculations obtained with Group 2 (low REEs content) did not converge to realistic solution for the mass balance of rocks and meteoric water. These unrealistic calculations indicate either erroneous partition coefficients of distribution REEs used for barite and fluid, or REEs variation related to inclusions of calcite and hematite in barite (REEs in calcite and hematite). Another explanation is a fluid migration from an area distant from the Seival such as a regional aquifer. The higher REEs contents (Figure 7B) of barite group (brt1) and liquid in Group 2 with low Ce/La ratio may suggest a different mixture than the Group 1 (REEs high content) and calculations succeed in finding several solutions with large errors. The most realistic solutions show a dominant fraction of meteoric water (99.97 – 99.99 %) and traces of rock (0.03 – 0.01%). In this case, the calculations include 8965 – 8878 volume of meteoric water and 1.1 – 2.8 volumes of pyroclastic rock (RFM48) and lamprophyric dike (LP225), respectively. Moreover, the calculation does not explain all the REEs in barite such as Gd, Nd, Sm, and Dy elements. These calculations reveal: i) a barite REEs composition possibly related to of pyroclastic rock (RFM48) or of lamprophyre dike (LP225) alteration, and ii) uncertainties related to the large volume of meteoric water and an accumulation of REEs in this water. This unrealistic accumulation of REEs has to be due to a low-temperature evaporation or hydrothermal boiling processes that increase major and trace elements in the residual water. Evaporation or hydrothermal boiling increases the content of major elements such as Ba^{2+} and SO_4^{2-} ions. Due to evaporation-hydrothermal boiling of water, the estimation of Ba and S through the composition of whole-rocks and plagioclase is likely overestimated. The REEs composition (Figure 7B) and calculations, despite the uncertainties, indicate distinct episodes of barite crystallization for Group 1 (rich in REEs; with Ce/La approximately 1.7) and Group 2 (poor in REEs; with Ce/La approximately 0.6). The source of REEs in Group 2 barite remains unclear. One possibility is low-temperature precipitation associated with fluid flow within a regional aquifer, providing a potential source of REEs, Ba, and S for these barites.

CONCLUSIONS

The presence of barite, hematite, and calcite veins indicates the dominance of fluids with SO_4^{2-} ions and represents the most recent low-temperature hydrothermal activity. This cooling trend and transition of HS_2 to HS^- and SO_4^{2-} -rich fluids can be linked to the intermixing of magmatic and meteoric hydrothermal water, which has been observed in comparable deposits from Camaquã Basin by Bongiolo et al. (2011) and Renac et al. (2014). In the Seival area, the transition from magmatic to meteoric fluid is linked to albitization and chloritization of volcanogenic deposits, which have copper-rich sulfides and barite. The inferred barite crystallization temperature (<157 °C) implies fault reactivation and penetration of meteoric-hydrothermal water. The Ba, S, and REEs chemical contents in barite and the absence of a Ce anomaly confirm that magmatic rocks and hydrothermal meteoric water interacted, rather than seawater. Calculation suggest that each mole of barite, was produced by alteration of 426 moles of andesite-labradorite from nearby volcanic rocks. The REEs mass balance confirms that barite, with higher REEs contents (Group 1), derives from alteration of pyroclastic rock (RFM48) or possibly lamprophyric dike (LP225; Lima and Nardi, 1998), while no realistic solution was found for Group 2. The balance between REEs from meteoric water, and magmatic rocks is taken into account. The ability to distinguish "parent minerals"

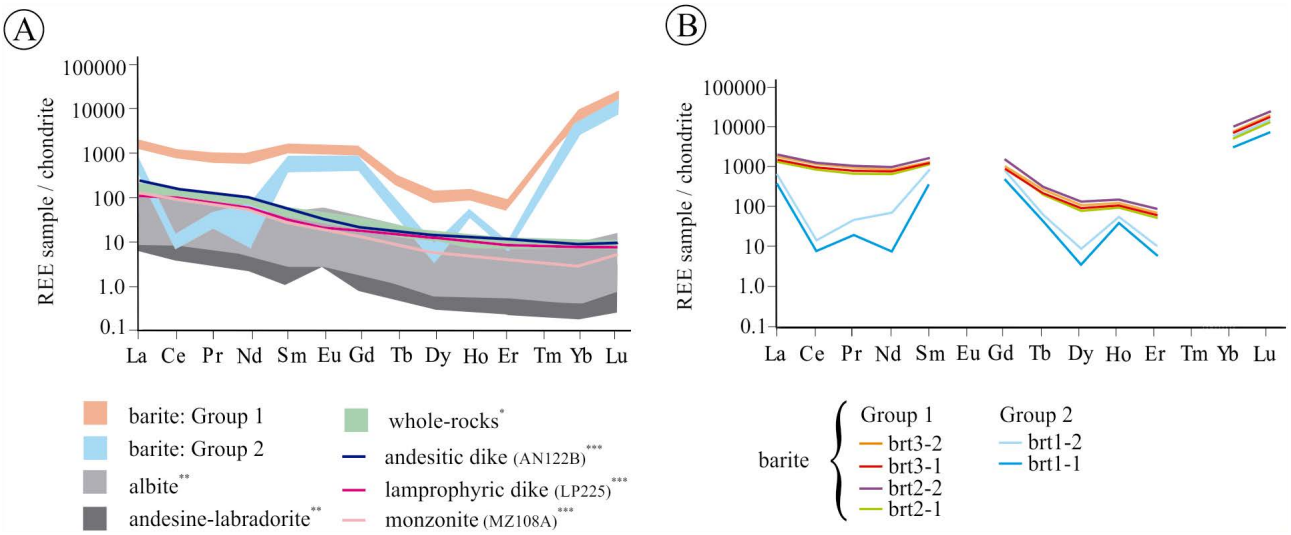

Figure 7. REEs of patterns normalized to chondrite (McDonough and Sun, 1995). (A) Comparison between Group 1 and Group 2 barite compositions, andesine-labradorite, albite, whole-rocks, andesitic dike, lamprophyric dike, and monzonite patterns. Data in green (*) from Lopes et al. (2014), gray and dark gray (**) from Lopes et al. (2019), and purple, pink and orange lines (***) from Lima and Nardi (1998) are plotted for comparison purposes. (B) Two patterns of barite with REEs enrichment, Group 1 and Group 2.

of barite with chemical compositions or the influence of a lamprophyric dike can aid in distinguishing active hydrothermal cells with potential base metal enrichment barite (Group 1) from barite (Group 2) that could be a result of a regional aquifer. Therefore, the major element and REEs compositions in barite represent a geochemical fingerprint of intense circulation and may serve as an indicator of the spatial correlation between mixing magmatic and meteoric fluids in an epithermal system.

ACKNOWLEDGMENTS

This study is the third part of the co-tutela doctoral thesis of Rodrigo Winck Lopes at Universidade Federal do Rio Grande do Sul and Université Côte d´Azur. We express our gratitude to the Conselho Nacional de Desenvolvimento Científico e Tecnológico (CNPq), Coordenação de Aperfeiçoamento de Pessoal de Nível Superior (CAPES), and the Programa Ciências Sem Fronteiras (Process number: 200081/2014-4) for financial support. We would like to thank the anonymous reviewers from Geologia USP, Série Científica for this revision. We would like to thank the anonymous reviewers from Brazilian Journal of Geology and Journal of South American Earth Science for the revision and suggestions of the withdrawal and recused version, respectively. We would like to thank Ana Maria Pimentel Mizusaki, Everton Marques Bongiolo, and Maria José Maluf de Mesquita for the revision and correction of an early version of this manuscript. Lastly, we thank the laboratory technician: Susan Drago, Denise Canarim, Edgar Bercht, Lucas Gomes and Lucas Jantsch. We would like to thank Marcelo Tatsch Lindenberg and Bruno Petracco de Miranda for their help in sampling and fieldwork.

REFERENCES

Almeida, F. F. M., Hasuy, Y. (1984). *O Pré-Cambriano do Brasil.* São Paulo: Edgard Blücher, 378 p.

Almeida, F. F. M., Brito Neves, B. B., Carneiro, C. D. R. (2000). The origin and evolution of South American platform. *Earth-Science Reviews*, 50, 77-111. https://doi.org/10.1016/S0012-8252(99)00072-0

Almeida, D. P. M., Chemale Jr., F., Machado, A. (2012). Late to post–orogenic Brasiliano–Pan–African volcano–sedimentary basins in the Dom Feliciano Belt, southernmost Brazil. In: Al–Juboury, A. I. (Ed.). *Petrology – New Perspectives and Applications. InTechOpen,* Chapter 5, p. 73-135. https://doi.org/10.5772/25189

Aries, S., Valladon, M., Polvé, M., Dupré, B. (2000). A routine method for oxide and hydroxide interference corrections in ICP-MS chemical analysis of environmental and geological samples. *Geostandard Newslet*, 24, 19-31. https://doi.org/10.1111/j.1751-908X.2000.tb00583.x

Baioumy, H. M. (2015). Rare earth elements, S and Sr isotopes and origin of barite from Bahariya Oasis, Egypt: Implication for the origin of host iron ores. *Journal of African Earth Sciences*, 106, 99-107. https://doi.org/10.1016/j.jafrearsci.2015.03.016

Barrett, T. J., Jarvis, I., Jarvis, K. E. (1990). Rare earth element geochemistry of massive sulfides sulfates and gossans on the Southern Explorer Ridge. *Geology*, 18, 583-586. https://doi.org/10.1130/0091-7613(1990)018<0583:REEGOM>2.3.CO;2

Barbieri, M., Mais, U., Tolomeo, L. (1982). Strontium geochemistry in the epithermal barite deposits from the Apuan Alps (Northern Tuscany, Italy). *Chemical Geology*, 35, 351-356. https://doi.org/10.1016/0009-2541(82)90011-0

Bettencourt, J. S. B. (1976). Minéralogie, inclusion fluides et isotopes stables de l'oxygène et du soufre de la Mine de Cuivre de Camaquã-RS (une étude préliminaire). In: *XXIX Congresso Brasileiro de Geologia*. Anais, p. 409-423. Ouro Preto: SBG.

Bongiolo, E. M., Renac, C., Mexias, A. S., Gomes, M. E. B., Ronchi, L. H., Patrier-Mas, P. (2011). Evidence of Ediacaran glaciation in southernmost Brazil through magmatic to meteoric fluid circulation in the porphyry-epithermal Au-Cu deposits of Lavras do Sul. *Precambrian Research*, 189, 404-419. https://doi.org/10.1016/j.precamres.2011.05.007

Breit, G. N., Simmons, E .C., Goldhaber, M. B. (1985). Dissolution of barite for the analysis of strontium isotopes and other chemical and isotopic variations using aqueous sodium carbonate. *Chemical Geology*, 52, 333-336. https://doi.org/10.1016/0168-9622(85)90043-0

Brimhall, G. H., Crerar, D. A. (1987). Ore fluids: magmatic to supergene. In: Ribbe, P. H. (Ed.), Thermodynamic modeling of geological materials minerals, fluids and melts. *Reviews in mineralogy*, 17, 235-321. https://doi.org/10.1515/9781501508950-010

Brito Neves, B. B., Fuck, R. A., Campanha, G. A. C. (2021). Basement inliers of the Brasiliano structural provinces of South America. *Journal Of South American Earth Sciences*, 110, 103392, p. 23. https://doi.org/10.1016/j.jsames.2021.103392

Camozzato, E., Toniolo, J. A., Laux, J. H. (2014). Metalogênese do Cinturão Dom Feliciano e Fragmentos Paleocontinentais associados (RS/SC). In: Silva, M. G., Rocha Neto, M. B., Jost, H., Kuyumjian, R. M. (Eds.). *Metalogênese das Províncias Tectônicas Brasileiras*. Belo Horizonte: Serviço Geológico do Brasil-CPRM, p. 517-556.

Censi, P., Mazzola, S., Sprovieri, M., Bonanno, A., Patti, B., Punturo, R., Spoto, S. E., Saiano, F. (2004). Rare earth elements distribution in seawater and suspended particulate of the Central Mediterranean Sea. *Chemistry and Ecology*, 20, 323-343. https://doi.org/10.1080/02757540410001727954

Censi, P., Inguaggiato, C., Chiavetta, S., Schembri, C., Censi, V., Falcone, E. E., Zuddas, P. (2017). The behaviour of zirconium, hafnium and rare earth elements during the crystallization of halite and other salt minerals. *Chemical Geology*, 453, 80-91. https://doi.org/10.1016/j.chemgeo.2017.02.003

Chang, L. L. Y., Howie, R. A., Zussman, J. (1996). Rock-Forming Minerals. Non-Silicates: Sulfates, Carbonates, Phosphates, Halides. *Geological Society*, London, p. 383. https://doi.org/10.1180/minmag.1996.060.400.20

Chemale Jr., F. (2000). Evolução Geológica do Escudo Sul-rio-grandense. In: Holz, M., De Ros, L. F. (Eds.). *Geologia do Rio Grande do Sul.* Porto Alegre: Universidade Federal do Rio Grande do Sul, p. 13-52.

Chiba, H., Sakai, H. (1985). Oxygen isotope exchange between dissolved sulfate and water at hydrothermal temperatures. *Geochimica et Cosmochimica Acta*, 49, 993-1000. https://doi.org/10.1016/0016-7037(85)90314-X

Chow, T. J., Goldberg, E. D. (1960). On the marine geochemistry of barium. *Geochimica et Cosmochimica Acta*, 20, 192-198. https://doi.org/10.1016/0016-7037(60)90073-9

Church, T. M., Bernat, M. (1971). Thorium and uranium in marine barite. *Earth and Planetary Science Letters*, 14, 139. https://doi.org/10.1016/0012-821X(72)90093-3

Church, T. M., Wolgemuth, K. (1972). Marine barite saturation. *Earth and Planetary Science Letters*, 15, 35-44. https://doi.org/10.1016/0012-821X(72)90026-X

De Toni, G. B., Monteiro, A., Tungo, E., Syangeve, L., Assis, N. F., Lopes, R. W., Tognoli, F. M. W. (2021). Diatremas da Formação Hilário nas minas do Seival, Bacia do Camaquã, sul do Brasil. *Pesquisas em Geociências*, 48(4), e110131. https://doi.org/10.22456/1807-9806.110131

Deer, W. A., Howie, R. A., Zussman, J. (2013). *An Introduction to the Rock Forming Minerals*. London: Mineralogical Society of Great Britain & Ireland, 3nd ed., p. 510. https://doi.org/10.1180/DHZ

Dill, H. G. (2015). Supergene Alteration of Ore Deposits: From Nature to Humans. *Elements*, 11, 201-206. https://doi.org/10.2113/gselements.11.5.311

Dulski, P. (1994). Interferences of oxide, hydroxide and chloride analyte species in the determination of rare earth elements in geological samples by inductively coupled plasma-mass spectrometry. *Fresenius' Journal of Analytical Chemistry*, 350, 194-203. https://doi.org/10.1007/bf00322470

Ehya, F. (2012). Rare earth element and stable isotope (O, S) geochemistry of barite from the Bijgan deposit, Markazi Province, Iran. *Mineralogy Petrology*, 104, 81-93. https://doi.org/10.1007/s00710-011-0172-8

Elderfield, H. (1988). The oceanic chemistry of the rare earth elements. *Philosophical Transactions of the Royal Society of London*, A325, 105-126. https://doi.org/10.1098/rsta.1988.0046

Fontana, E., Mexias, A. S., Renac, C., Nardi, L. V. S., Lopes, R. W., Gomes, M. E. B., Barats, A. (2017). Hydrothermal alteration of volcanic rocks in Seival Mine Cu-mineralization - Camaquã Basin - Brazil (Part I): Chloritization process and geochemical dispersion in alteration halos. *Journal of Geochemical Exploration*, 177, 45-60. https://doi.org/10.1016/j.gexplo.2017.02.004

Fontana, E., Renac, C., Mexias, A. S., Barats, A., Gerbe, M. C., Lopes, R. W., Nardi, L. V. S. (2019). Mass balance and origin of fluids associated to smectite and chlorite/smectite alteration in Seival Mine Cu-Mineralization - Camaquã Basin - Brazil (Part II). *Journal of Geochemical Exploration*, 196, 20-32. https://doi.org/10.1016/j.gexplo.2018.10.001

Fulignati, P. (2020). Clay Minerals in Hydrothermal Systems. *Minerals*, 10(10), 919. https://doi.org/10.3390/min10100919

Gastal, M. C., Lafon, J. M., Ferreira, F. J. F., Magro, F. U. S., Remus, M. V. D., Sommer, C. A. (2006). Reinterpretação do Complexo Intrusivo Lavras do Sul - RS, de acordo com os sistemas vulcano-plutônicos de subsidência. Parte I: Geologia, geofísica e geocronologia ($^{207}Pb/^{206}Pb$ e $^{206}Pb/^{238}U$). *Brazilian Journal of Geology*, 36, 109-124.

Gastal, M. C., Ferreira, F. J. F., Cunha, J. U., Esmeris, C., Koester, E., Raposo, M. I. B., Rossetti, M. M. M. (2015). Lavras granite emplacement and gold mineralization during the development of the post-collisional volcano-plutonic center, west of the Sul-rio grandense Shield: geophysical and structural data. *Brazilian Journal of Geology*, 45, 217-241. https://doi.org/10.1590/23174889201500020004

Goldberg, E. D., Somayajulu, B. L. K., Galloway, J., Kaplan, I. R., Faure, G. (1969). Differences between barites of marine and continental origins. *Geochimica Cosmochimica Acta*, 33, 287-289. https://doi.org/10.1016/0016-7037(69)90145-8

Green, D. H. (1980). Island arc and continent building magmatism - A review of petrogenic models based on experimental petrology and geochemistry. *Tectonophysics*, 63, 367-385. https://doi.org/10.1016/0040-1951(80)90121-3

Guichard, F., Church T. M., Treuil, M., Jaffrezic, H. (1979). Rare earths in barites: distribution and effects on aqueous partitioning. *Geochimica Cosmochimica Acta*, 43, 983-997. https://doi.org/10.1016/0016-7037(79)90088-7

Hanor, J. S. (2000). Reviews in Mineralogy & Geochemistry - Sulfate Minerals. In: Alpers, N., Jambor, J. L., Nordstrom, D. K. (Eds.). *Barite-celestine geochemistry and environments of formation*. Washington: Mineralogical Society of America, p. 193-275.

Hartmann, L. A., Chemale Jr., F., Philipp, R. P. (2007). Evolução Geotectônica do Rio Grande do Sul no Pré-Cambriano. In: Iannuzzi, R., Frantz, J. C. (Eds.). *50 anos de Geologia: Instituto de Geociências.* Porto Alegre: Universidade Federal do Rio Grande do Sul, p. 99-123.

Hoefs, J. (2009). *Stable Isotope Geochemistry*. Berlin: Springer, p. 286. https://doi.org/10.1007/978-3-319-78527-1

Hogdahl, O. T., Melsom, S., Bowen, V. T. (1968). Neutron activation analysis of lanthanide elements in sea water. In: Baker, R. A. (Ed.). Trace inorganics in water. *Journal of the American Chemical Society*, 73(19), p. 308. https://doi.org/10.1021/ba-1968-0073.ch019

Hövelmann, J., Putnis, A., Geisler, T., Schmidt, B. C., Golla-Schindler, U. (2010). The replacement of plagioclase feldspars by albite: observations from hydrothermal experiments. *Contributions to Mineralogy and Petrology*, 159, 43-59. https://doi.org/10.1007/s00410-009-0415-4

Hueck, M., Oyhantçabal, P., Philipp, R. P., Basei, M. A. S., Siegesmund, S. (2018). The Dom Feliciano Belt in Southern Brazil and Uruguay. In: Siegesmund, S., Basei, M., Oyhantçabal, P., Oriolo, S. (Eds.). *Geology of Southwest Gondwana*. Springer, Regional Geology Reviews, p. 267-302. https://doi.org/10.1007/978-3-319-68920-3_11

Inguaggiato, C., Censi, P., Zuddas, P., Londono, J. M., Chacon, Z., Alzate, D., Brusca, L., D'Alessandro, W. (2015). Geochemistry of REE, Zr and Hf in a wide range of pH and water composition: the Nevado del Ruiz volcano-hydrothermal system (Colombia). *Chemical Geology*, 417, 125-133. https://doi.org/10.1016/j.chemgeo.2015.09.025

Inguaggiato, C., Garzon, G., Burbano, V., Rouwet, D. (2017). Geochemical processes assessed by Rare Earth Elements fractionation at "Laguna Verde" acidic-sulphate crater lake (Azufral volcano, Colombia). *Applied Geochemistry*, 79, 65-74. https://doi.org/10.1016/j.apgeochem.2017.02.013

Inguaggiato, C., Iñiguez, E., Peiffer, L., Kretzschmar, T., Brusca, L., Mora-Amador, R., Ramirez, C., Bellomo, S., Gonzalez, G., Rouwet, D. (2018). REE fractionation during the gypsum crystallization in hyperacid sulphate-rich brine: The Poás Volcano crater lake (Costa Rica) exploited as laboratory. *Gondwana Research*, 59, 87-96. https://doi.org/10.1016/j.gr.2018.02.022

Inoue, A., Meunier, A., Patrier–Mas, P., Rigault, C., Beaufort, D., Vieillard, P. (2009). Application of chemical geothermometry to low–temperature trioctahedral chlorites. *Clays and Clay Minerals*, 57, 371-382. https://doi.org/10.1346/CCMN.2009.0570309

Jarvis, K. E., Gray, A. L., McCurdy, E. (1989). Avoidance of spectral interference on europium in inductively coupled plasma mass spectrometry by sensitive measurement of the doubly charged ion. *Journal of Analytical Atomic Spectrometry*, 4, 743-747. https://doi.org/10.1039/JA9890400743

Jarvis, K. E., Gray, A. L., Houk, R. S. (1992). *Handbook of Inductively Coupled Plasma Mass Spectrometry.* Glasgow: Blackie, p. 380.

Jamieson, J. W., Hanningtone, M. D., Tivey, M. K., Hansteen, T., Williamson, N. M., Stewart, M., Fietzke, J., Butterfield, D., Frische, M., Allen, L., Cousens, B., Langer, J. (2016). Precipitation and growth of barite within hydrothermal vent deposits from the Endeavour Segment, Juan de Fuca Ridge. *Geochimica et Cosmochimica Acta*, 173, 64-85. https://doi.org/10.1016/j.gca.2015.10.021

Johannesson, K. H., Palmore, D., Fackrell, J., Prouty, N. G., Swarzenski, P. W., Chevis, D. A., Telfeyan, K., White, C. D., Burdige, D. J. (2017). Rare earth element behavior during groundwater seawater mixing along the Kona Coast of Hawaii. *Geochimica et Cosmochimica Acta*, 198, 229-258. https://doi.org/10.1016/j.gca.2016.11.009

Janikian, L., Almeida, R. P., Trindade, R. I. F., Fragoso-Cesar, A. R. S., D´Agrella-Filho, M. S., Dantas, E. L., Tohver, E. (2008). The continental record of Ediacaran volcano-sedimentary successions in southern Brazil and their global implications. *Terra Nova*, 20, 259-266. https://doi.org/10.1111/j.1365-3121.2008.00814.x

Janikian, L., Almeida, R. P., Fragoso-Cesar, A. R. S., Martins, V. T. S., Dantas, E. L., Tohver, E., McReath, I., D'Agrella-Filho, M. S. (2012). Ages (U-Pb SHRIMP and LA ICPMS) and stratigraphic evolution of the Neoproterozoic volcano-sedimentary successions from the extensional Camaquã Basin, Southern Brazil. *Gondwana Research*, 21, 466-482. https://doi.org/10.1016/j.gr.2011.04.010

Jurkovic, I., Garasic, V., Hrvatovic, H. (2010). Geochemical characteristics of barite occurrences in the Palaeozoic complex of south-eastern Bosnia and their relationship to the barite deposits of the mid-Bosnian Schist Mountain. *Geologia Croatica*, 63, 241-258. https://doi.org/10.4154/gc.2010.20

Kameda, J., Ujiie, K., Yamaguchi, A., Kimura, G. (2011). Smectite to chlorite conversion by frictional heating along a subduction-zone thrust. *Earth and Planetary Science Letters*, 305, 161-170. https://doi.org/10.1016/j.epsl.2011.02.051

Li, Y. H. (1982). A brief discussion on the mean oceanic residence time of elements. *Geochimica et Cosmochimica Acta*, 46, 2671-2675. https://doi.org/10.1016/0016-7037(82)90386-6

Li, X., Zhang, C., Almeev, R. R., Holtz, F. (2020). GeoBalance: An Excel VBA program for mass balance calculation in geosciences. *Geochemistry*, 80(2), 125629. https://doi.org/10.1016/j.chemer.2020.125629

Lima, E. F., Nardi, L. V. S. (1998). The Lavras do Sul Shoshonitic Association: implications for origin and evolution of neoproterozoic shoshonitic magmatism in southernmost Brazil. *Journal of South American Earth Sciences*, 11, 67-77. https://doi.org/10.1016/S0895-9811(97)00037-0

Lima, E. F. L., Sommer, C. A., Nardi, L. V. S. (2007). O vulcanismo Neoproterozóico-Ordoviciano no escudo sul-riograndense: os ciclos vulcânicos da Bacia do Camaquã. In: Iannuzzi, R., Frantz, J. C. (Eds.). *50 anos de Geologia: Instituto de Geociências*. Porto Alegre: Universidade Federal do Rio Grande do Sul, pp. 79-97.

Liz, J. D., Lima, E. F., Nardi, L. V. S. (2009). Avaliação de fontes magmáticas de séries shoshoníticas pós-colisionais com base na normalização pela Associação Shoshonítica de Lavras do Sul - aplicação de Sliding Normalization. *Brazilian Journal of Geology*, 39, 55-66. https://doi.org/10.25249/0375-7536.20093915566

Longerich, H. P., Fryer, B. J., Strong, D. F., Kantipuly, C. J. (1987). Effects of operating conditions on the determination of the rare earth elements by inductively coupled plasma-mass spectrometry (ICP-MS). *Spectrochim Acta B*, 42, 75-92. https://doi.org/10.1016/0584-8547(87)80051-4

Lopes, R. W., Fontana, E., Mexias, A. S., Gomes, M. E. B., Nardi, L. V. S., Renac, C. (2014). Caracterização petrográfica e geoquímica da sequência magmática da Mina do Seival, Formação Hilário (Bacia do Camaquã - Neoproterozoico), Rio Grande do Sul, Brasil. *Pesquisas em Geociências*, 41, 51-64. https://doi.org/10.22456/1807-9806.78035

Lopes, R. W., Mexias, A. S., Philipp, R. P., Bongiolo, E. M., Renac, C., Bicca, M. M., Fontana, E. (2018). Au-Cu-Ag mineralization controlled by brittle structures in Lavras do Sul Mining District and Seival Mine deposits, Camaquã Basin, southern Brazil. *Journal of South American Earth Sciences*, 88, 197-215. https://doi.org/10.1016/j.jsames.2018.08.017

Lopes, R. W., Renac, C., Mexias, A. S., Nardi, L. V. S., Fontana, E., Gomes, M. E. B., Barats, A. (2019). Mineral assemblages and temperature associated with Cu enrichment in the Seival area (Neoproterozoic Camaquã Basin of Southern Brazil). *Journal of Geochemical Exploration*, 201, 56-70. https://doi.org/10.1016/j.gexplo.2019.03.010

Martin, E. E., Macdougall, J. D., Herbert, T. D., Paytan, A., Kastner, M. (1995). Strontium and neodymium isotopic analysis of marine barite separates. *Geochimica et Cosmochimica Acta*, 07, 1353-1361. https://doi.org/10.1016/0016-7037(95)00049-6

Martinez-Ruiz, F., Paytan, A., Gonzalez-Muñoz, M. T., Jroundi, F., Abad, M. M., Lam, P. J., Horner, T. J., Kastner, M. (2020). Barite Precipitation on Suspended Organic Matter in the Mesopelagic Zone. *Frontiers in Earth Science*, 8, 567714. https://doi.org/10.3389/feart.2020.567714

McDonough, W. F., Sun, S. S. (1995). The composition of the earth. *Chemical Geology*, 120, 223-253. https://doi.org/10.1016/0009-2541(94)00140-4

Mehnert, K. R., Büsch, W. (1981). The Ba content of K feldspar megacrysts in granites, a criterion for their formation. *Neues Jahrbuch Mineralogie Abhandlungen*, 140, 21-252. https://doi.org/10.1007/s00410-009-0444-z

Michard, G., Alberede, F., Michard, A., Minster, J. F., Charlou, J. L., Tan, N. (1984). Chemistry of solutions from 13°N East Pacific Rise hydrothermal site. *Earth and Planetary Science Letters*, 67, 297-307. https://doi.org/10.1016/0012-821X(84)90169-9

Michard, A. (1989). Rare earth element systematics in hydrothermal fluids. *Geochimica et Cosmochimica Acta*, 53, 745-750. https://doi.org/10.1016/0016-7037(89)90017-3

Morgan, J. W., Wandless, G. A. (1980). Rare earth element distribution in some hydrothermal minerals: evidence for crystallographic control. *Geochimica et Cosmochimica Acta*, 44, 973-980. https://doi.org/10.1016/0016-7037(80)90286-0

Ohmoto, H. (1972). Systematics of sulfur and carbon in hydrothermal ore deposits. *Economic Geology*, 67, 551-579. https://doi.org/10.2113/gsecongeo.67.5.551

Oriolo, S., Hueck, M., Oyhantçabal, P., Goscombe, B., Wemmer, K., Siegesmund, S. (2018). Shear zones in Brasiliano-Pan-African belts and their role in the amalgamation and break-up of Southwes Gondwana. In: Siegesmund, S., Basei, M. A. S., Oyhantçabal, P., Oriolo, S. (Eds.). *Geology of Southwest Gondwana*. Berlim: Springer Nature, Regional Geology Reviews, p. 593-613. https://doi.org/10.1007/978-3-319-68920-3_22

Oyhantçabal, P., Siegesmund, S., Wemmer, K. (2011). The Rio de la Plata Craton, a review of units, boundaries, ages and isotopic signature. *International Journal of Earth Sciences*, 100, 201-220. https://doi.org/10.1007/s00531-010-0580-8

Paim, P. S. G., Chemale Jr., F., Lopes, R. C. (2000). A Bacia do Camaquã. In: Holz, M., de Ros, L. F. (Eds.). *Geologia do Rio Grande do Sul*. Porto Alegre: Universidade Federal do Rio Grande do Sul, p. 231-374.

Paim, P. S. G., Chemale Jr., F., Wildner, W. (2014). Estágios evolutivos da Bacia do Camaquã (RS). *Ciência e Natura*, 36, 183-193. http://dx.doi.org/10.5902/2179460X13748

Pereira, D. R., Macambira, M. J. B., Pires, K. C. J, Lago, S. B. (2021). Isotopic study of the Pb-Zn (Cu-Ag) Santa Maria Deposit, Caçapava do Sul Region, Rio Grande do Sul, Brazil. *Brazilian Journal of Geology*, 51(1), 1-16. https://doi.org/10.1590/2317-4889202120200091

Piper, D. Z. (1974). Rare-Earth Elements in the Sedi Cycle: A Summary. *Chemical Geology*, 14, 285-304. https://doi.org/10.1016/0009-2541(74)90066-7

Pirajno, F. (2009). *Hydrothermal processes and mineral systems*. Berlin: Springer, p. 1250. https://doi.org/10.1007/978-1-4020-8613-7

Philipp, R. P., Pimentel, M. M., Chemale Jr., F. (2016). Tectonic evolution of the Dom Feliciano Belt in Southern Brazil: Geological relationships and U-Pb geochronology. *Brazilian Journal of Geology*, 46, 83-104. https://doi.org/10.1590/2317-4889201620150016

Raut, N. M., Huang, L-S, Aggarwal, S. K., Lin, K-C (2005a). Mathematical Correction for Polyatomic Isobaric Spectral Interferences in Determination of Lanthanides by Inductively Coupled Plasma Mass Spectrometry. *Journal of the Chinese Chemical Society*, 52, 589-597. https://doi.org/10.1002/jccs.200500087

Raut, N. M., Huang, L-S, Lin, K-C, Aggarwal S. K. (2005b). Uncertainty propagation through correction methodology for the determination of rare earth elements by quadrupole based inductively coupled plasma mass spectrometry. *Analytica Chimica Acta*, 530, 91-103. https://doi.org/10.1016/j.aca.2004.08.067

Reischl, J. L. (1978). Mineralizações cupriferas associadas a vulcânicas na Mina do Seival., In: *XXX Congresso Brasileiro de Geologia*. Anais, p. 1568-1582. Recife: SBG.

Remus, M. V. D., Hartmann, L. A., McNaughton, N. J., Groves, D. I., Reischl, J. L. (2000). Distal Magmatic-Hydrothermal Origin for the Camaquã Cu (Au-Ag) and Santa Maria Pb, Zn (Cu-Ag) Deposits, Southern Brazil. *Gondwana Research*, 03, 155-174. https://doi.org/10.1016/S1342-937X(05)70094-0

Renac, C., Mexias, A. S., Gomes, M. E. B., Ronchi, L. H., Nardi, L. V. S., Laux, J. H. (2014). Isotopic fluid changes in a Neoproterozoic porphyry epithermal system: the Uruguay mine, southern Brazil. *Ore Geology Reviews*, 60, 146-160. https://doi.org/10.1016/j.oregeorev.2013.12.016

Ronchi, L. H., Lindenmayer, Z. G., Bastos Neto, A. C., Murta, C. R. (2000). O stockwork e a zonação do minério sulfetado no arenito inferior da Mina Uruguai, RS. In: Ronchi, L. H., Lobato, A. O. C. (Eds.). *Minas do Camaquã, um estudo multidisciplinar*. São Leopoldo: Universidade do Vale do Rio dos Sinos / Fundação de Amparo à Pesquisa do Estado do Rio Grande do Sul, p. 165-190. Available at: https://www.researchgate.net/publication/262100260_O_stockwork_e_a_zonacao_do_minerio_sulfetado_no_arenito_inferior_da_Mina_Uruguai_RS. Accessed on: nov 17, 2025.

Schijf, J., Byrne, R. H. (2004). Determination of SO4ß1 for yttrium and the rare earth elements at I= 0.66 m and t= 25 °C - Implications for YREE solution speciation in sulphate-rich waters. *Geochimica et Cosmochimica Acta*, 68, 2825-2837. https://doi.org/10.1016/j.gca.2003.12.003

Schleicher, A. M., van der Pluijm, B. A., Warr, L. N. (2012). Chlorite-smectite clay minerals and fault behavior: New evidence from the San Andreas Fault Observatory at Depth (SAFOD) core. *Lithosphere*, 04, 209-220. https://doi.org/10.1130/L158.1

Seal II, R. R. (2006). Sulfur isotope geochemistry of sulfide minerals. *Reviews in Mineralogy and Geochemistry*, 61, 633-677. https://doi.org/10.2138/rmg.2006.61.12

Shabani, M. B., Akagi, T., Masuda, A. (1992). Preconcentration of trace Rare Earth Elements in sea water by complexation with bis (2-ethylhexyl) hydrogen phosphate and 2-ethylhexyl dihydrogen phosphate adsorbed on a C18 cartridge and determination by inductively coupled plasma mass spectrometry. *Analytical Chemistry*, 64, 737-743. https://doi.org/10.1021/ac00031a008

Sillitoe, R. H. (2010). Porphyry copper systems. *Economic Geology*, 105, 3-41. https://doi.org/10.2113/gsecongeo.105.1.3

Smirnova, E. V., Mysovskaya, I. N., Lozhkin, V. I., Sandimirova, G. P., Pakhomova, N. N., Smagunova, A. A. (2006). Spectral interferences from polyatomic barium ions in inductively coupled plasma mass spectrometry. *Journal of Applied Spectroscopy,* 73, 911-917. https://doi.org/10.1007/s10812-006-0175-0

Sorrell, C. A. (1962). Solid state formation of barium, strontium and lead feldspars in clay-sulfate mixtures. *The American Mineralogist*, 47, 291-309. Available at: http://www.minsocam.org/ammin/AM47/AM47_291.pdf. Accessed on: nov 17, 2025.

Toniolo, J. A., Remus, M. V. D., Macambira, M. J. B., Moura, C. A. V. (2004). Metalogênese do Depósito de Cobre Cerro dos Martins, RS, Revisão e Geoquímica Isotópica de Sr, S, O e C. *Pesquisas em Geociências*, 31, 41-67. https://doi.org/10.22456/1807-9806.19573

Vaughan, D. J., Craig, J. R. (1997). Sulfide ore mineral stabilities, morphologies, and intergrowth textures. In: Barnes, H. L. (Ed.). *Geochemistry of hydrothermal ore deposits, third edition.* New York: John Willey & Sons, p. 367-434.

Vaughan, D. J., Corkhill, C. L. (2017). Mineralogy of sulfides. *Elements*, 13, 81-87. https://doi.org/10.2113/gselements.13.2.81

Wildner, W., Ramgrag, G. E., Lopes, R. C., Iglesias, C. M. F. (2006). *Mapa Geológico do Estado do Rio Grande do Sul, scale 1:750.000* - Projeto Geologia do Brasil ao Milionésimo - Programa Geologia do Brasil. Porto Alegre: CPRM. Available at: https://rigeo.sgb.gov.br/bitstream/doc/10301/2/Geologico_MDT.pdf. Accessed on: nov 17, 2025.

Zarasvandi, A., Zaheri, N., Pourkaseb, H., Chrachi, A., Bagheri, H. (2014). Geochemistry and fluid-inclusion microthermometry of the Farsesh barite deposit, Iran. *Geologos*, 20, 201-214. https://doi.org/10.2478/logos-2014-0015

Zhao, W., Zong, K., Liu, Y., Hu, Z., Chen, H., Li, M. (2019). An effective oxide interference correction on Sc and REE for routine analyses of geological samples by inductively coupled plasma-mass spectrometry. *Journal of Earth Science*, 30, 1302-1310. https://doi.org/10.1007/s12583-019-0898-5